Jpn. J. Appl. Phys. Vol. 35 (1996) pp. 1786–1797
Part 1, No. 3, March 1996

Quantitative Deconvolution of Photomodulated Thermoreflectance Signals from Si and Ge Semiconducting Samples

Andreas MANDELIS* and Robert E. WAGNER

Photothermal and Optoelectronic Diagnostics Laboratory, Department of Mechanical Engineering, University of Toronto, Toronto M5S 1A4, Canada

(Received September 14, 1995; accepted for publication January 17, 1996)

A variety of photomodulated thermoreflectance (PMTR) data have been obtained for two germanium wafer samples (one crystalline and the other ion-implanted and unannealed), and three silicon wafer samples (one crystalline, unimplanted; the other implanted and flash-annealed; and the third an amorphous thin layer). Physically different mechanisms contributing to the PMTR signals have been formulated theoretically for these materials. For the crystalline and implanted-annealed samples it was found that the PMTR signal has two main components, one due to temperature modulation (thermal wave); the other due to the free-carrier density modulation (the Drude effect). For the ion-implanted-unannealed and amorphous materials two components were found to be dominant: one due to the thermal wave; the other due to the band-filling of localized gap states. The two component mechanisms were validated in a quantitative manner by curve-fitting experimental PMTR frequency-response data, while taking into account the photocurrent (PC) responses of the samples. As a result, unambiguous deconvolution of the electron-hole plasma or trapped-carrier contribution and the thermal-wave component to the PMTR signal were obtained throughout the frequency range 1 kHz–1.6 MHz.

KEYWORDS: photomodulated thermoreflectance, semiconductors, thermal-wave, photocurrent, band-filling, signal deconvolution

1. Introduction

In recent years, the photomodulated thermoreflectance (PMTR) technique has been used quite extensively to qualitatively characterize the electronic/thermal transport properties of crystalline and ion-implanted semiconductors.[1–9] The basis of the PMTR technique is as follows: A semiconductor wafer is illuminated with an intense ($> 10^4\,\mathrm{Wcm}^{-2}$), modulated, monochromatic pump beam - usually from a laser - which is capable of exciting electrons from the valence band to the conduction band. This optical excitation causes the reflectance of the sample to be modulated at the modulation frequency of the pump beam. The modulated reflectance of the semiconductor is detected via a second laser beam, the probe, which is co-incident with the pump beam on the sample.

There are several mechanisms possibly contributing to the PMTR signal from a semiconductor sample in response to super-bandgap optical illumination: The non-radiative de-excitation of the photo-carriers causes the temperature modulation of the sample (a thermal wave), resulting in thermoreflectance modulation termed the thermoreflectance effect;[3] the change in the free-carrier density induced by the intensity-modulated pump beam in turn modulates the reflectance via the Drude effect,[3] and through the band-filling of the conduction and valence band states;[10] the optically-induced modulation of the surface built-in electric field causes reflectance modulation via the Franz–Keldysh mechanism, a phenomenon known as the photoreflectance (PR) effect;[11] finally, if there is a large density of localized states in the energy gap, which is the case for amorphous and ion-implanted semiconductors, the optical band-filling of localized gap-states can also change the sample modulated reflectance.[12–14] The relative sizes of the various effects detailed above depend upon several factors, such as the pump and probe photon energies, the intensity of the pump beam, the thermal and electronic properties of the sample, the modulation frequency, and the spot-size of the pump beam.

In this work, several Ge and Si semiconductor samples were studied using the PMTR technique, with additional insights from photocurrent (PC) measurements. A detailed three-dimensional theoretical/numerical model of the PMTR signal was also developed. Based on this model, a quantitative method for estimating the components of competing electronic and thermal mechanisms was developed and applied to crystalline, ion-implanted and amorphous samples. The method derives its signal deconvolution capability from the determination of internally self-consistent, best theoretical fits to a series of PMTR frequency responses under a wide range of pump laser-beam spotsizes. As a result, the dominant signal generation mechanisms for crystalline (c-) Si and Ge, implanted (im-) Ge, and amorphous (a-) Si were unambiguously and quantitatively resolved for the first time.

2. Theoretical Model of the PMTR Effect

The basic relation for the PMTR signal takes into account that there are two main and physically different components to be considered: a thermal component (ΔR_T) due to lattice absorption and heating and a (free or trapped) carrier component (ΔR_N):

$$\Delta R = \Delta R_\mathrm{T} + \Delta R_\mathrm{N} \tag{1}$$

where R is the sample reflectance, and ΔR is the modulated reflectance. It is convenient to write:

$$\Delta R_\mathrm{T} = \frac{\partial R}{\partial T}\,\Delta T\,, \tag{2}$$

and

$$\Delta R_\mathrm{N} = \frac{\partial R}{\partial N}\,\Delta N\,, \tag{3}$$

*E-mail address: mandelis@me.utoronto.ca

where $\partial R/\partial T$ is the temperature reflectance coefficient, $\partial R/\partial N$ is the carrier reflectance coefficient, ΔT is the modulated temperature rise, and ΔN is the photomodulated excess-carrier density. In general, when calculating ΔR for an air/sample interface, one must take into account the depth dependence of ΔT and ΔN. Under superband-gap excitation and in the vast majority of cases, Wagner and Mandelis[15] have shown that it is valid to replace ΔT and ΔN in eqs. (2) and (3) with ΔT_0 and ΔN_0, the surface thermomodulation and excess-carrier modulation values, respectively.

2.1 *The Carrier Component of ΔR*

For a semiconductor the value of $\partial R/\partial N$ can be estimated from the Drude model:[16]

$$\frac{\partial R}{\partial N} \approx -\frac{\lambda^2 e^2}{2\pi^2 \epsilon_0 m^* c^2} \frac{n-1}{n(n+1)^3}. \tag{4}$$

Here, λ is the probe wavelength, e is the electronic charge, ϵ_0 is the permittivity of free space, c is the speed of light in vacuum, n is the refractive index, and $1/m^* = 1/m_e^* + 1/m_h^*$, where m_e^* is the electron effective mass, and m_h^* is the hole effective mass. Equation (4) is based on the valid assumption that k, the extinction coefficient, is much smaller than n, and that the sample is a "good" crystalline material (or, $\omega_p \gg 1/\tau_s$, where ω_p is the optical angular frequency of the probe radiation, and s is the carrier scattering/relaxation time). The derivation of Equation (4) for c-Si and c-Ge, assumes that the PMTR signal component due to the PR effect is negligible, which is reasonable for the experimental situation where high excitation fluence is employed.[17–19] Also, it was assumed that the optical band-filling of extended states is not significant, which is consistent with independent calculations.[20]

For im-Ge and a-Si, the value for $\partial R/\partial N$ was expected to be related to the band-filling of localized gap-states, rather than to the Drude effect. Since the nature of the gap-states was not known, no reliable estimate for the magnitude of $\partial R/\partial N$ could be made for these materials. On the other hand, modeling performed for the related situation of the optical band-filling of extended states in the conduction and valence bands of im-Ge indicated that $\partial R/\partial N$ should be greater than zero when the probe photon energy is much greater than the energy gap.[10] For a-Si the probe photon energy was also much greater than the damage layer mobility gap. It was thus expected that $\partial R/\partial N$ would also be positive.

For the c-Ge and c-Si samples, the theoretical value of ΔN was obtained by solving the carrier diffusion equation:

$$\frac{\partial(\Delta N)}{\partial t} = D\nabla^2(\Delta N) - \frac{\Delta N}{\tau} + S(r,z,t) \tag{5}$$

where ΔN is the modulated photo-carrier density , D is the average of the electron and hole diffusion coefficients (an approximation to the ambipolar value), τ is the band-to-band recombination time, and $S(r,z,t)$ is the source function for the photo-carrier generation. The source term represents the response of the sample to a focussed pump beam with a radially-symmetric Gaussian profile, and is of the form:

$$S(r,z,t) = \frac{\alpha P}{\pi w^2} e^{-\alpha z} e^{-r^2/w^2} e^{i\omega t} \tag{6}$$

where α is the optical absorption coefficient of the pump beam, P is the peak number of photons absorbed by the sample each second, w is the $1/e$ radius of the pump beam, ω is the angular modulation frequency, z is the distance into the sample, and r is the radial coordinate.

Equation (5) was solved using the Hankel transform technique,[21] and the boundary conditions used to determine ΔN took into account both surface recombination and the finite thickness of the c-Ge and c-Si samples. In general, $\Delta N(r,z)$ is complex:

$$\Delta N(r,z) = \Delta N_r + i\Delta N_i \tag{7}$$

The carrier lifetime τ of eq. (5) was assumed to be independent of ΔN, an assumption which is usually only valid when ΔN is small. Since the value of ΔN can be quite large during a PMTR experiment, due to the high intensity of the pump beam, τ may become a function of ΔN, for instance, via an Auger mechanism.[22]

Since the band-filling of gap-states was expected to dominate the Drude effect in the damage layer of the im-Ge and a-Si samples, the value of ΔN to be employed should be a function of the population of non-equilibrium carriers trapped in the localized gap-states. Thus, eq. (5) does not strictly apply, and one must generalize the problem to finding the carrier population of the localized states in the gap as a function of energy. Since this type of problem cannot be realistically tackled, due to uncertainties regarding the nature and the behavior of the gap-states in the im-Ge, eq. (5) was employed to determine the population of the states responsible for the band-filling effect, and an effective recombination time was assumed for these states. With regard to boundary conditions, the im-Ge damage layer and the a-Si surface thin-film layer were assumed to be in contact with a semi-infinite, insulating substrate. This assumption reflects the expectation that the trapped carriers in the damage layers were not able to easily move into the crystalline substrate material, and was justified a *posteriori* through the model fit to the data .

2.2 *The Thermal Component of ΔR*

Although $\partial R/\partial T$ can, in principle, be theoretically calculated,[15] it is much more convenient to determine this parameter experimentally. $\partial R/\partial T$ has been tabulated in the literature for c-Si and for a number of visible wavelengths, but no data exist for c-Ge, im-Ge or a-Si. Therefore, in this work the foregoing parameter was quantified experimentally. The theoretical value of ΔT was obtained by solving the heat diffusion equation:

$$\frac{\partial(\Delta T)}{\partial t} = \beta_s \nabla^2(\Delta T) + F(r,z,t) \tag{8}$$

where ΔT is the modulated temperature (peak-to-peak), β_s is the sample thermal diffusivity, and $F(r,z,t)$ is the heat source function. The heat source function is composed of two components, one related to the almost-instantaneous intraband relaxation of hot photo-carriers, and the other related to the non-radiative interband recombination of the thermalized photo-carriers; these two

components will be denoted as F_1 and F_2, respectively.

The intraband heating component is[23]

$$F_1(r,z,t) = (h\nu - E_g)\frac{\beta_s}{k_s}\frac{\alpha P}{\pi w^2} \times e^{-\alpha z} e^{-r^2/w^2} e^{iwt} \quad (9)$$

where $h\nu$ is the pump photon energy, E_g is the energy gap, and k_s is the sample thermal conductivity. Also, the interband heating component is[23]

$$F_2(r,z,t) = E_g \eta \frac{\beta_s}{k_s}\frac{\Delta N(r,z,t)}{\tau} \quad (10)$$

where η is the non-radiative quantum efficiency (the percentage of recombination energy converted to heat-effectively one for c-Ge and im-Ge), and ΔN is the modulated free-carrier density. Since F_2 depends upon the carrier recombination/transport properties of the sample, ΔR_T provides information regarding both the thermal and the electronic properties of the sample.

Equation (8) was also solved using the Hankel transform method.[21] With regard to boundary conditions, the c-Ge and c-Si samples were considered to be of finite thickness, with the front surface in contact with a semi-infinite body of air, and the back surface insulated; surface carrier recombination was taken into account. The im-Ge and a-Si samples were modeled as a thin layer upon a semi-infinite substrate, with the front surface in contact with a semi-infinite body of air. In general, $\Delta T(r,z)$ is complex:

$$\Delta T(r,z) = \Delta T_r + i\Delta T_i \quad (11)$$

2.3 *Calculation of ΔR from ΔN and ΔT*

Once the ΔN and ΔT components have been theoretically determined, eq. (1) can be used to determine the amplitude and phase of the ΔR phasor:

$$\Delta R(r,z) = \Delta R_r + i\Delta R_i \quad (12)$$

where

$$\Delta R_r = \frac{\partial R}{\partial T}\Delta T_r + \frac{\partial R}{\partial N}\Delta N_r, \quad (13)$$

and

$$\Delta R_i = \frac{\partial R}{\partial T}\Delta T_i + \frac{\partial R}{\partial N}\Delta N_i, \quad (14)$$

Overall, the modulated reflectance has a peak-to-peak amplitude of:

$$|Re\Delta R(r,z,t)| = \sqrt{{\Delta R_r}^2 + {\Delta R_r}^2} \quad (15)$$

and the *phase lag* is given by:

$$\theta_R = \tan^{-1}\left(-\frac{\Delta R_i}{\Delta R_r}\right) \quad (16)$$

In addition to calculating $\Delta R(r,z)$, simulation of the experimental PMTR signal requires that one take into account the intensity profile of the probe beam. If both the pump and probe beams are at normal incidence, and they are concentric Gaussian beams, the reflectance modulation sampled by the probe beam is:

$$< \Delta R >= \frac{2}{R_p^2}\int_0^\infty \Delta R(r)\, e^{-r^2/{R_p}^2}\, r dr \quad (17)$$

where R_p is the $1/e$ radius of the probe beam. In fact, if $R_p \ll w$, then $< \Delta R > \approx \Delta R\ (r=0)$, and modeling the PMOR signal is simplest in this case.

3. Materials and Experimental

The two Ge samples of this study were identical except for the fact that the implanted sample had a thin damage layer on its surface. The c-Ge wafer was cut from a single-crystal boule, yielding a < 111 > surface orientation. The Ge melt had been doped with gallium, creating a p-type material with a resistivity of about 15 Ω cm. The thickness of the wafer was about 200 μm, and the diameter was 5 cm. One face of the substrate was polished to a mirror-smooth finish, while the other face had a matte appearance. The im-Ge sample was fabricated by implanting a crystalline substrate with 100 keV phosphorus ions to a dose of $10^{16}\,cm^{-2}$. According to published ion-range tables,[24] these implant parameters should create an amorphous damage layer with a thickness of about 0.13 μm. Three different samples of silicon were also studied, two crystalline samples and an amorphous thin film. The two crystalline samples had the following processing history: First, a < 100 >, n-type wafer with a thickness of 385 μm and a resistivity of 100 Ω cm was ion-implanted over half of its surface with arsenic ions. The implantation dose was $10^{15}\,cm^{-2}$ at 180 keV. The wafer then was flash-annealed at 950°C for 20 s to remove the lattice damage and electrically activate the dopant. Following this annealing, the implanted side of the wafer had a new surface-layer resistivity of 10 Ω cm. The non-implanted Si will be henceforth labeled as c-Si1, and the implanted-annealed sample will be labeled c-Si2. The a-Si sample was obtained from Mitel Semiconductors (Bromont, Quebec, Canada) and consisted of a 0.8 μm layer of amorphous silicon deposited on a crystalline silicon substrate at 570°C by a low-pressure chemical vapor deposition process. This deposition temperature was close to the critical level (670°C) at which the film would be expected to be polycrystalline.

PMTR measurements were performed using the apparatus shown in Fig. 1. The pump beam was focussed onto the sample using a 3-cm focal length achromat, and attained a minimum 1/e radius of 5.7 μm beyond this lens. The 3-cm lens was mounted on an x–y–z micrometer translation system, allowing the lens/sample separation distance (z-axis) to be varied in order to alter the pump

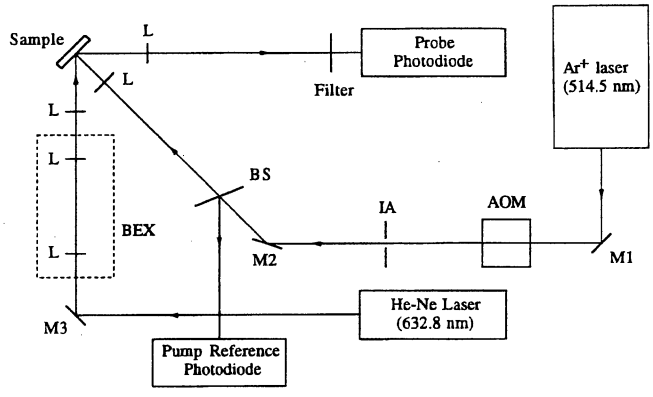

Fig. 1. Schematic diagram of PMTR apparatus. AOM – acousto-optic modulator; BEX – beam expander; BS – beam splitter; IA – iris aperture; M – mirror; L – lens

spot-size on the sample. The lens could be translated in the x–y plane, normal to the propagation direction of the pump beam, in order to precisely position the laser spot on the sample.

The probe beam was obtained from an unpolarized, 2 mW He–Ne laser, operating at a wavelength of 632.8 nm. The probe was expanded five times, and then focussed onto the sample with a 7.3 cm focal length achromat lens. The focal point of the probe beam was made to coincide with the pump spot by adjusting the lens/sample separation distance. The minimum $1/e$ probe radius was measured to be 6.3 μm. The probe beam did not strike the sample at normal incidence, but had an angle of incidence of 28°; therefore, the beam projection on the surface was an ellipse with a long axis about 13% longer than the short axis. The output signal from the probe detector was input to a lock-in analyzer. Two different lock-in models were employed: For modulation frequencies from 100 Hz to 160 kHz, the EG&G Model 5204 was used, and for frequencies from 100 kHz to 1.6 MHz, the EG&G Model 5202 high-frequency instrument was utilized.

After raw PMTR data were obtained, the amplitude of the experimental signal was converted to an absolute quantity, $\Delta R/R$ per watt of absorbed pump power, and the experimental PMTR phase was converted to an absolute phase (0 to 360°) relative to the excitation waveform. The normalization of the raw PMTR data was made possible by the complete calibration of the experimental system, and the normalization scheme ensured that both amplitude and phase data would be free of artifacts due to the frequency response of the measuring system.

In order to obtain the carrier lifetime, the transverse modulated photocurrent (PC) was measured as a function of modulation frequency. Metal contacts were made on opposite edges of the sample, and electrical leads were attached. A d.c. voltage was applied to the sample via the external conductors, resulting in a field which was oriented parallel to the illuminated surface. Then, the sample was excited with a modulated laser beam, which was defocused so that the sample was illuminated in a uniform manner. The PC flowing through the sample was probed by measuring the a.c. voltage drop across a small reference resistor placed in series with the sample, Fig. 2. The carrier lifetime was extracted from PC frequency response data using the method described by Warabisako *et al.*[25]

4. Results

4.1 *Determination of the temperature reflectance coefficient*

The temperature reflectance coefficient was obtained as follows. A sample was mounted on the end of an aluminum rod. The rod had a resistance wire coiled around it, and when a dc current was passed through the wire, the rod slowly heated up. The reflectance of the sample was monitored with a He–Ne laser, which reflected from the sample to a monitoring photodiode. The sample temperature was estimated via a thermocouple probe also mounted on the end of the aluminum rod.

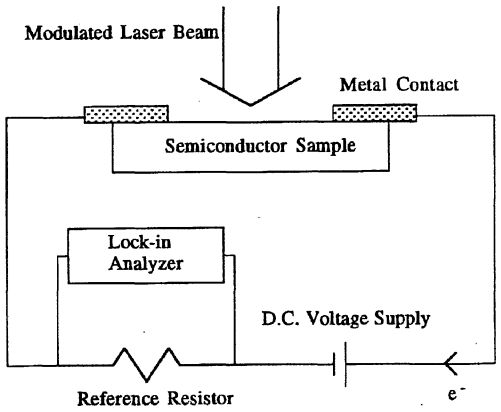

Fig. 2. Schematic diagram of experimental apparatus used for measuring the transverse modulated photocurrent.

At the start of a test, the initial temperature T_1 of the sample was recorded; then, the photodiode reflectance signal was monitored until it was steady, after which sample heating commenced. The reflectance signal was monitored until a new temperature (T_2) was reached, about 50°C above room temperature. For a given temperature difference of $\Delta T = T_2 - T_1$, the value of $\partial R/\partial T$ can easily be shown to be:

$$\frac{\partial R}{\partial T} = \frac{R}{\Delta T}\left[\frac{V(T_2)}{V(T_1} - 1\right], \tag{18}$$

where R is the nominal reflectance of the sample, and $V(T_j)$ is the photodiode signal at temperature T_j. Due to the very small signal changes which were induced during a typical test, the measurement of $\partial R/\partial T$ was repeated several times for each sample, and an average value was calculated.

In order to test the accuracy of the method used to determine $\partial R/\partial T$ an initial experiment was performed on a c-Si sample, since the value of $\partial R/\partial T$ for c-Si at 632.8 nm is available in the literature.[26] The present technique yielded a value of $6.0 \times 10^{-5}\,\mathrm{K}^{-1}$, as compared to the literature value of $4.2 \times 10^{-5}\,\mathrm{K}^{-1}$; thus, it was assumed that the heater method overestimated the value of $\partial R/\partial T$ by 43%. Taking into account the above-mentioned assumption as a systematic error, the value of $\partial R/\partial T$ determined for the c-Ge was $1.85 \times 10^{-4}\,\mathrm{K}^{-1}$, and the value for the im-Ge was $6.1 \times 10^{-5}\,\mathrm{K}^{-1}$. Owing to the large scatter of the He-Ne laser beam by the a-Si sample, no accurate experimental estimate was possible for the $\partial R/\partial T$ value of this sample. The average estimate was $(4.2 \pm 0.9) \times 10^{-5}\,\mathrm{K}^{-1}$.

Photocurrent spectra were also obtained for all the samples. The resulting signals from the crystalline wafers were almost three orders of magnitude higher than those from the implanted and amorphous surfaces, a result consistent with the expected fast trapping time constant and the low mobility for trapped carriers in defect-rich semiconductors. Figure 3 shows the frequency dependence of the photocurrent signal from the c-Ge sample. A similar plot was obtained for c-Si. Following standard analyses[25] a carrier lifetime $\tau = 10\,\mu$s was extracted from the "knee" frequency ω^* in this plot for c-Ge. The c-Si1 and c-Si2 samples behaved like typical crystalline

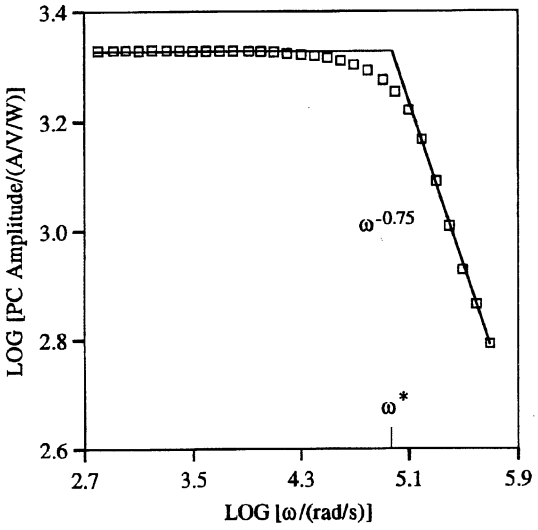

Fig. 3. Modulated photocurrent (per watt of absorbed pump power, per unit applied dc bias) vs. angular modulation frequency for c-Ge. Details: $\lambda = 514.5$ nm; sample resistance = 937 Ω; dc bias = 0.2 V.

semiconductors, with free-carrier lifetimes in the range from 16 μs (c-Si1) to 28 μs (c-Si2). Surface recombination velocities (SRVs) were estimated[23] in the 100–1000 m/s range for these samples, using the slopes of the decreasing high-frequency signal in semilogarithmic plots similar to Fig. 3. For c-Ge Fig. 3 gave a power dependence on frequency equal to $\omega^{-0.75}$. This suggests[23] a value of SRV in the range 10–100 m/s. The respective data from the im-Ge and the a-Si did not follow the expected behavior, but instead exhibited a photocurrent curve dominated by localized trapping states: It has been found that photo-carriers in materials like amorphous Ge and Si are trapped in times shorter than 10^{-11} s,[27,28] followed by a much longer recombination time span. In general, it was not possible to assign a single characteristic relaxation time to the im-Ge sample.

4.2 *PMTR signal transient studies*

Opsal *et al.*[3] reported PMTR measurements on c-Si for which the signal was observed to vary slowly as a function of time. In particular, the PMTR signal was found to increase or decrease monotonically from its initial value to a steady-state value which was different from the initial value. The observed temporal effects where attributed to the trapping of photo-carriers by surface states, and it was found that the temporal effects could be eliminated by growing a thermal oxide layer on the sample surface, a treatment which is known to passivate certain surface states related to Si dangling bonds.

For the c-Ge and c-Si samples, no transient effects were observed for absorbed pump intensities as high as 3.5×10^5 Wcm^{-2}, at 10 kHz. On the other hand, the im-Ge and a-Si PMTR signals tended to decrease with time when the absorbed intensity was above 4.7×10^5 Wcm^{-2} at 10 kHz. Disordered materials like im-Ge and a-Si have a large density of localized gap-states which are known to undergo metastable, light-induced changes, such as the Staebler–Wronski (S–W) effect.[29] In the present case, the light-induced changes in the PMTR signal were usually fully reversible at room temperature, indicating that a relatively small activation energy was required for returning a sample to its dark-state; therefore, it does not seem likely that the observed temporal changes in the PMTR signal were due to a typical S–W effect, which is not surprising since both im-Ge and a-Si samples did not contain hydrogen, which is important when the S–W effect occurs in a-Si. Graf *et al.*[30] have observed photo-induced changes in the properties of a-Si:H which they believe are precursors to the S–W effect; they hypothesized that illumination caused dangling bonds to form which were not subsequently locked into a metastable state via hydrogen attachment. This precursor to the S–W effect may have been responsible for the temporal effects evidenced for the im-Ge and the a-Si samples.

Since the thermal component of the PMTR signal for the im-Ge and a-Si samples should have been quite insensitive to the occupation of the localized gap-states in the thin surface damage layers, it is likely that their PMTR transient behavior was actually related to the band-filling component.

4.3 *PMTR signal intensity dependence*

The PMTR signal was measured as a function of absorbed pump intensity. Measurements were performed at 1 MHz. The pump wavelength was 514.5 nm, the probe wavelength was 632.8 nm, and the 1/e pump radius was 5.7 μm.

For the c-Ge material at 10 kHz (Fig. 3), the PMTR amplitude increased linearly with intensity at lower powers ($I^{1.03}$), and with a weak supra-linearity at higher powers ($I^{1.16}$). This behavior was explained[31] by assuming that the c-Ge PMTR signal was dominated by the thermal component, and that a combination of Auger carrier recombination and the temperature dependence of the thermal conductivity yielded the supra-linear behavior at elevated powers. According to the model presented in ref. 31, the intensity dependence of the Drude component of the PMTR signal should be strongly sub-linear when Auger recombination is dominant while the intensity dependence of the thermal component should be weakly supra-linear. The calculations performed in ref. 31 also indicated that the Auger recombination effect should be very important at the higher power levels of Fig. 4. Therefore, if the Drude signal component was dominant for the c-Ge, this material would have yielded a strongly sub-linear intensity dependence, rather than the supra-linear behavior which was actually observed. An additional piece of evidence indicating the dominance of the thermal component over the Drude component in the c-Ge was that the phase was usually in the range 0 to −45°, indicating thermal domination ($\partial R/\partial T > 0$), while a PMTR signal dominated by the Drude effect would have possessed a phase near −180°, since ($\partial R/\partial N < 0$).

The c-Si2 sample exhibited behavior similar to that of im-Ge. On the other hand, for the c-Si1 the PMTR amplitude increased linearly with intensity at low optical powers ($\sim I^{1.07}$), and with significant supra-linearity at higher powers ($\sim I^{1.48}$). The Auger mechanism is

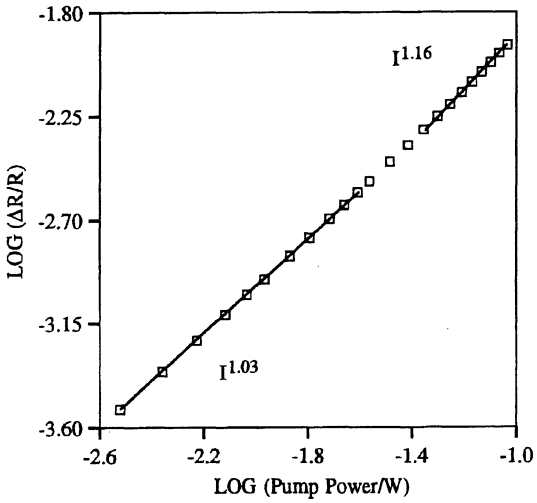

Fig. 4. Normalized PMTR amplitude vs. absorbed pump power for c-Ge, at 10 kHz. Details: pump $\lambda = 514.5$ nm; probe $\lambda = 632.8$ nm; nominal $1/e$ pump radius $= 5.7$ μm; nominal $1/e$ probe radius $= 6.3$ μm.

not capable of yielding such strong non-linearities.[31] It is possible that the SRV was also a function of the free-carrier density for the c-Si1, and that this effect was responsible for the observed supra-linearity. The intensity dependence of the PC further indicated that the carrier lifetime and/or the SRV was dependent on carrier density for this sample. An additional possible source of the supra-linearity is, of course, the temperature dependence of the thermal conductivity and diffusivity.

4.4 *Signal modulation frequency dependence and mechanism deconvolution*

For all PMTR modulation frequency varying experiments, the pump wavelength was 514.5 nm, and the probe wavelength was 632.8 nm. Data were taken at a minimum of four different $1/e$ pump radii: 5.7, 8.4, 15.5, and 23.3 μm. The frequency was varied from 10^3 to 1.6×10^6 Hz. Due to the limited bandwidth of the lock-in analyzers, each high-frequency scan consisted of two separate experiments each employing a different lock-in analyzer. The high-f scans were only performed with pump radii of 5.7 and 23.3 μm.

Since the pump beam radius has a significant effect upon the deconvolution of the frequency response of the PMTR signal, this parameter was well characterized. The spatial profiles of the focused pump and probe beams were determined, and the beam radii were carefully controled during PMTR measurements. The pump radius was varied by adjusting the position of the focusing lens with respect to the sample, leading to a degree of uncertainty regarding the exact pump spot-size. Therefore, when PMTR signal, $S(f)$, data were fitted to the theoretical model, the pump radius was one of the adjustable parameters. With regard to the fidelity of the experimental data, the normalized $S(f)$ curves were usually quite smooth, but in situations where the points deviated somewhat from a smooth curve, a three-point smoothing algorithm was employed.

The curve-fitted amplitude plots were absolutely calibrated for the incident laser fluence, and the curves were converted to their true, absolute values ($\Delta R/R$ per watt of absorbed pump power) by using the multiplying factors provided in some of the figure captions to be presented below. With regard to the curve-fitting procedure, a sample's properties were obtained from the literature, or by independent measurement. For the c-Ge and c-Si samples it was quite straightforward to obtain many of the required material properties, since they have been widely tabulated in the literature. On the other hand, for the im-Ge and the a-Si samples it was not possible to obtain many of the required physical parameters with a high degree of accuracy, due to the fact that electronic relaxation and transport are not very well understood in disordered materials, and because the behavior of a particular sample is strongly dependent upon its processing history.

For the crystalline samples, the only material parameter which was not well characterized was the Drude reflectance coefficient (DRC). Using eq. (4), the DRC for c-Ge was estimated to be $-3.0 \times 10^{-29}\,\mathrm{m}^3$, taking into account that the Ge refractive index (n) is 4.6,[32] and the reduced mass (m^*) is 0.11 times the electron mass, m_0.[33] For c-Si the DRC was estimated to be $-2.5 \times 10^{-29}\,\mathrm{m}^3$, using[32] $n = 4.2$ and[33] $m^* = 0.16 m_0$. It should be kept in mind that the theoretical carrier diffusion equation, eq. (5), *does not take into account Auger recombination*, which was known to be present during the PMTR optical intensity-dependence measurements on the c-Ge and c-Si. This omission was accounted for, to some extent, by the fact that the value of the SRV was used as an adjustable parameter during the fitting of the experimental PMTR data to the theoretical model. To rigorously account for Auger recombination in the carrier diffusion equation, the non-linear diffusion equation must be solved by numerical means, which is very complicated for the three-dimensional form of the carrier diffusion equation. The effects of Auger recombination for the one-dimensional carrier and heat diffusion equations have been considered elsewhere.[31]

Overall, the following criteria were used to obtain the best-fit parameters for mechanism deconvolution: 1) The theoretical and experimental PMTR $S(f)$ amplitude curves had to match in terms of shape, and to a lesser degree, in terms of absolute magnitude. 2) The theoretical and experimental $S(f)$ phase curves had to match well in an absolute sense. 3) The fit-value of the pump radius had to be within 40% of the nominal value. Usually, the error was less than 25%, except when the nominal radius was below 10 μm. 4) The SRV had to be within the range indicated by the photocurrent data, and the DRC had to be within a factor of five of the nominal theoretical value. 5) The *same set of parameters* had to yield good curve-fits *for all of the different pump radii employed.*

With respect to the uniqueness of the optimal set of best-fit parameters (pump radius, SRV, and DRC), due to the fact that the fitting routine required agreement with entire sets of data, each obtained with a different (and measured) laser beam radius, and since both of the other fitting parameters were known to a certain degree from either theoretical or experimental photocurrent

considerations, it is estimated that the chosen best-fits were within 20% of their "true" values. *The deviation of the best-fit laser spotsize from the measured values was used as a criterion of the uncertainty in the quantitative contribution of a particular mechanism (electronic or thermal) in the signal deconvolution process.* The parameters used to obtain the $S(f)$ curve-fits for the c-Ge and c-Si samples are presented in Table I. With regard to the data in this table, the SRVs were adjustable parameters, and their fit-values were within the range indicated by the frequency response of the transverse photocurrent. The recombination times were also obtained from the photocurrent data. The temperature reflectance coefficient was measured as described in §4.1.

Data were obtained over the range 1 kHz to 1.6 MHz. Figure 5 shows the data obtained with the nominal pump radius of 5.7 μm. Both amplitude and phase fits are excellent over the entire frequency range for both crystalline samples. The data also yielded an excellent quality curve-fit for the $1/e$ pump radius of 23.3 μm. Regarding the use of literature values for the only non-measured parameters in Table I (carrier diffusion coefficient, pump absorption coefficient, sample energy gap, and the thermophysical properties), their values are very well established for c-Si and c-Ge.[32,34] Intentional variations of up to 5% in these parameters gave best-fit values of the pump radius, SRV and DRC well within the 20% uncertainty of their "true" values discussed above. Any variations in the sample reflectance at the pump or probe wavelengths from their literature values,[32] tended to rigidly shift the amplitude curves vertically. This resulted in simple re-definitions of the multiplying factors (theory) and had no effect on the values of the calculated best-fit parameters. Table II shows the best-fitted and nominal pump radii for the various scans performed for the samples c-Ge, c-Si1 and c-Si2. The fitted radii were generally larger than the nominal values, but the discrepancies tended to decrease as the radius increased.

For the im-Ge and a-Si samples, however, a significant number of material properties were not well characterized. The thermal conductivities of amorphous and crystalline Ge are quite different: im-Ge is likely to have a thermal conductivity somewhere between the two extremes presented by the crystalline and amorphous materials. In addition, although the Drude effect is normally quite negligible in disordered materials (due to the fast trapping of photo-carriers), disordered materials seem to provide a signal component which is related to the filling of localized gap-states, states which are very difficult to model accurately. Nevertheless, it was found

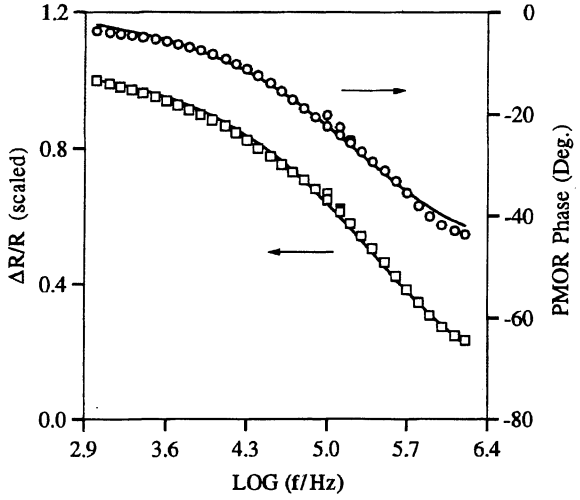

(a)

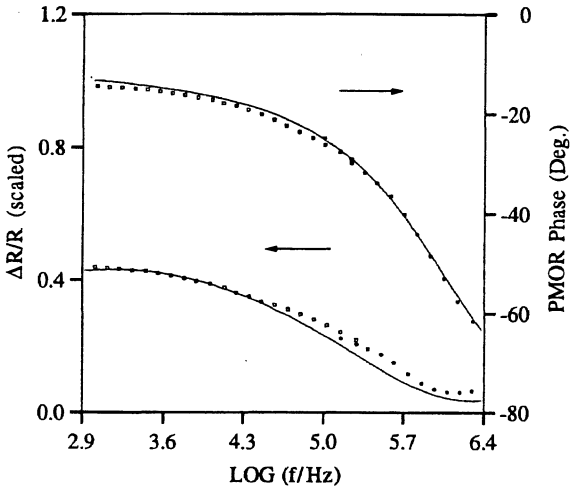

(b)

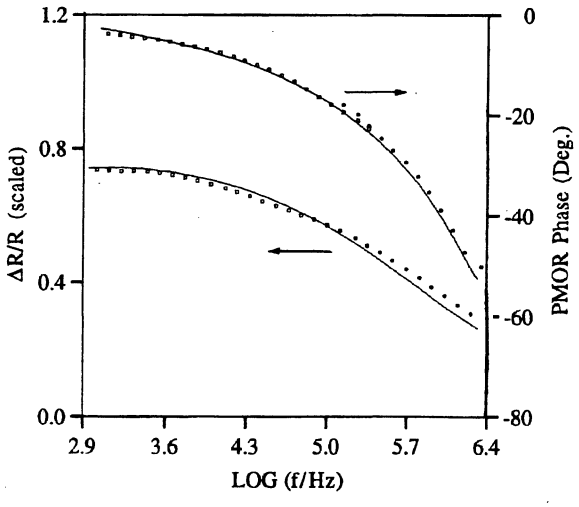

(c)

Fig. 5. (a) PMTR amplitude (□) and phase (o) vs. modulation frequency for c-Ge; the nominal $1/e$ pump radius is 5.7 μm, and the best-fit radius is 7.5 μm. The solid lines are theoretical fits. Multiplying factors to convert the PMTR amplitude to $\Delta R/R$ per watt of absorbed power are 0.147 (experiment) and 0.13 (theory). The absorbed pump power was 14 mW, and the experimental data had one cycle of smoothing. (b) Same as (a) for c-Si1. Best-fit radius was 7.0 μm. Multiplying factors are 0.011 (experiment) and 0.0078 (theory). The absorbed pump power was 66 mW and the experimental data had two cycles of smoothing. (c) Same as in (a) and (b) for c-Si2. Best-fit radius was 7.14 μm. Multiplying factors are 0.020 (experiment) and 0.0136 (theory). The absorbed pump power was 152 mW and the experimental data had two cycles of smoothing.

Table I. Physical parameters used to fit c-Ge and c-Si experimental $S(f)$ data to the theoretical model of §2.

	c-Ge	c-Si1	c-Si2
Surface recombination velocity (m/s)[a]	10	30	500
Recombination time (s)[b]	10^{-5}	1.6×10^{-5}	2.8×10^{-5}
Carrier diffusion coefficient (m^2/s)[c]	6.5×10^{-3}	2.4×10^{-3}	2.4×10^{-3}
$\partial R/\partial N$ @ 632.8 nm (m^3)[a,d]	-3.0×10^{-29}	-8.0×10^{-29}	-8.0×10^{-29}
Pump absorption coefficient (m^{-1})	6.0×10^{7}	1.46×10^{6}	1.46×10^{6}
Pump photon energy (eV)	2.4	2.4	2.4
Sample energy gap (eV)[e]	0.66	1.1	1.1
Reflectance @ 632.8 nm[e]	0.48	0.35	0.35
Reflectance @ 514.5 nm[e]	0.50	0.38	0.38
$\partial R/\partial T$ @ 632.8 nm (K^{-1})[b]	1.85×10^{-4}	4.2×10^{-5}	4.2×10^{-5}
Thermal conductivity (W/m·K)[c]	59	148	148
Specific heat (J/kg·K)[c]	310	691	691
Density (kg/m^3)[c]	5324	2328	2328
Sample thickness (m)[b]	0.206×10^{-3}	0.385×10^{-3}	0.385×10^{-3}

a) fit parameter b) measured c) Ref. 34 d) Eq. 4 e) Ref. 32

Table II. Normal and fitted $1/e$ pump radii for the c-Ge, c-Si1 and c-Si2 $S(f)$ data. Probe radius: 6.3 μm.

Normal radius (μm)	Fitted radius (μm)		
	c-Ge	c-Si1	c-Si2
5.7	7.6	7.9	9.0
8.4	9.4	9.2	9.5
15.5	19.3	16.1	15.6
23.3	28.5	21.0	20.8
34.4	39.6		
45.6	51.1		

that adequate $S(f)$ fits could be obtained for the im-Ge and a-Si by judiciously adjusting the electronic transport properties and the carrier reflectance coefficient. The im-Ge sample was considered to consist of two homogeneous layers, a surface layer of amorphous Ge, and a bulk layer of c-Ge. In reality, there was a gradual transition from amorphous to crystalline material, but the abrupt-change model was assumed to be adequate, since the thermal diffusion length was much greater than the thickness of the implanted layer ($< 1\mu$m). Therefore, the damage layer was extremely thermally thin, and the signal was not expected to be very sensitive to the exact nature of the near-surface region. The a-Si sample was by its fabrication a thin film.

When an initial attempt was made to fit the experimental $S(f)$ data to the theoretical model, assuming that only a thermal component was present, an acceptable fit was impossible. Subsequently, when a Drude component was included in the fitting procedure, *the sign of the carrier reflectance coefficient had to be made positive* in order for acceptable fits to be obtained. Since the Drude reflectance coefficient is usually negative (see ref. 16 for exceptions), and it was expected to be insignificant compared to the thermal-wave contribution anyway, due to the very high defect/trap densities in these materials, a different carrier-related PMTR component was required and hypothesized to exist: the band-filling of localized gap-states. This assumption was also consistent with the fact that the carrier reflectance coefficient for the band-filling effect should be positive for the probe wavelength employed.[12–14]

Table III. Physical parameters used to fit im-Ge and a-Si experimental $S(f)$ data to the theoretical model of §2.

	im-Ge	a-Si
Surface recombination velocity (m/s)[a]	0	0
Recombination time (s)[a]	10^{-7}	10^{-7}
Carrier diffusion coefficient (m^2/s)[b]	2.9×10^{-5}	1.6×10^{-5}
$\partial R/\partial N$ @ 632.8 nm (m^3)[c]	4.9×10^{-28}	3.0×10^{-29}
Pump absorption coefficient (m^{-1})	5.3×10^{7} [36]	1.44×10^{7} [40]
Pump photon energy (eV)	2.4	2.4
Sample energy gap (eV)	0.66[e]	1.6[39]
Reflectance @ 632.8 nm	0.46[36]	0.40[40]
Reflectance @ 514.5 nm	0.48[36]	0.44[40]
$\partial R/\partial T$ @ 632.8 nm (K^{-1})[f]	6.1×10^{-5}	4.2×10^{-5}
Thermal conductivity (W/m·K)	13[g]	35[38]
Specific heat (J/kg·K)	310[e]	691[38]
Density (kg/m^3)	5324[e]	2328
Layer thickness (m)	0.134×10^{-6}	0.8×10^{-6}

a) assumed b) Ref. 35 c) fit parameter d) same as c-Ge
e) measured f) Ref. 37 g) calculated, ref. 24

The parameters used to obtain the $S(f)$ curve-fits for the im-Ge and a-Si are presented in Table III. In order to model the trapped-carrier signal component, it was necessary to know the recombination time and carrier diffusion coefficient for the localized carriers, and the band-filling reflectance coefficient. Unfortunately, it is not possible to define a single carrier lifetime in disordered materials, since the lifetime is time dependent. Nevertheless, a carrier lifetime of 10^{-7} s was chosen for both samples; this value is both less than the lifetime in the c-Ge and c-Si substrates (10^{-5} s), and much longer than the trapping time in im-Ge and a-Si (10^{-11} s). The SRV was set to 0 m/s: since the implanted and amorphous layers were very thin ($< 1\mu$m) compared to the plasma diffusion length ($\sim 30\mu$m),[2] the SRV was effectively included in the carrier lifetime. With regard to the carrier diffusion coefficient (CDC) for the trapped carriers, it was noted that in a-Si the CDC is about 225 times less than in c-Si;[35] since Ge and Si share many similarities, it was assumed that the CDC in the im-Ge was also 225 times less than in the c-Ge. The band-filling reflectance coefficient was used as a fitting parameter, and it was adjusted until good fittings were obtained; note that using the band-filling reflectance coefficient as a fitting parameter helped to compensate for any errors made in estimating the values of the carrier lifetime, CDC, and SRV. The specific heat and density were assigned values known to be valid for c-Ge and polysilicon.[38] The energy

gap of im-Ge was assumed to be the same as for c-Ge; that of a-Si was assumed to be[39] 1.6 eV. The a-Si optical properties were obtained from Aspnes *et al.*[40] The thickness of the implanted layer in im-Ge was calculated from tabulated ion-implantation data.[24] Any variations in these parameters by more than 10–12% tended to yield best-fit pump-beam radii values over 40% of the nominal value, in violation of criterion 3, and were thus discarded.

Figure 6 shows the frequency dependent data obtained with the nominal pump radius of 5.7 μm. The amplitude fits are excellent over the entire frequency range. The phase fits are very good, although increasing discrepancy between theory and experiment became noticeable at the high-frequency extreme. This may be due to inhomogeneous recombination time and/or carrier diffusion coefficient depth profiles in the sample.[41] Similar data obtained with larger laser beam radii were of a similar quality to those obtained for the smallest radius of 5.7 μm. Table IV shows the best-fitted and nominal pump radii for five different $S(f)$ scans. The fitted radii were generally larger than the nominal values, but the discrepancies between the two values tended to decrease as the radius increased. Just as in the case of the crystalline samples, the theoretical model of the PMTR effect could well explain the major features and trends in the experimental data sets from the implanted and amorphous semiconductors.

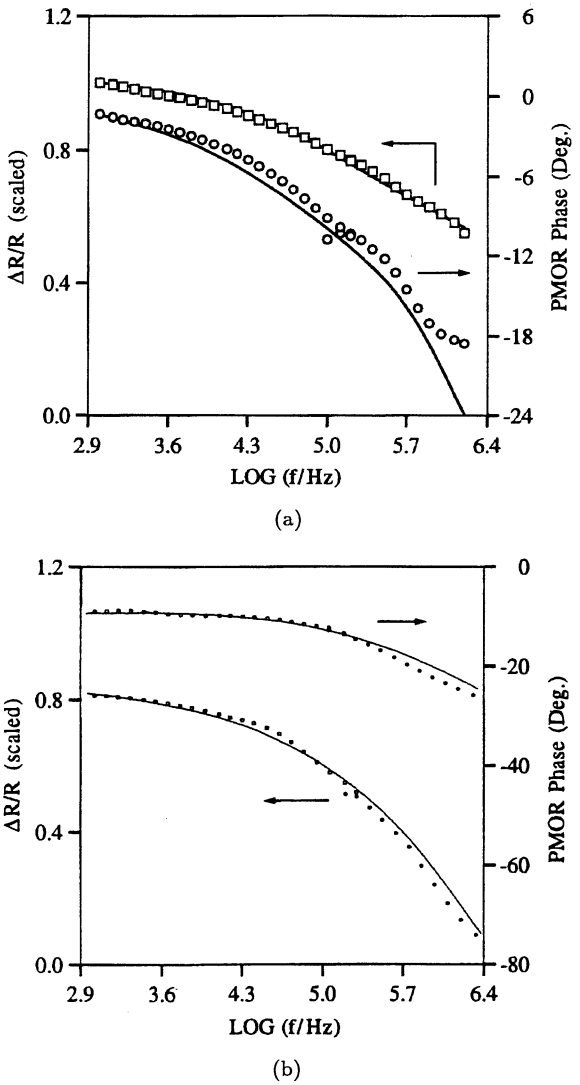

Fig. 6. (a) PMTR amplitude (□) and phase (o) vs. modulation frequency for im-Ge; the nominal $1/e$ pump radius is 5.7 μm, and the best-fit radius is 8.7 μm. The solid lines are theoretical fits. Multiplying factors to convert the PMTR amplitude to $\Delta R/R$ per watt of absorbed power are 0.102 (experiment) and 0.0844 (theory). The absorbed pump power was 20.7 mW, and the experimental data had two cycles of smoothing. b) Same as in (a) for a-Si. Best-fit radius was 7.13 μm. Multiplying factors are 0.090 (experiment) and 0.056 (theory). The absorbed pump power was 28.2 mW, and the experimental data had two cycles of smoothing.

Table IV. Nominal and fitted $1/e$ pump radii for the im-Ge and a-Si $S(f)$ data. Probe radius: 6.3μm.

Nominal radius (μm)	Fitted radius (μm)	
	im-Ge	a-Si
5.7	7.1	7.1
8.4	9.1	6.8
15.5	17.8	16.6
23.3	28.9	23.8

5. Discussion

The intensity dependence of the photocurrent indicated the presence of Auger recombination effects in the crystalline semiconductors at high excitation fluences. Corroborating theoretical modeling[31] shows that Auger recombination yields a Drude (free-carrier) PMTR signal with a strongly sub-linear intensity dependence, and a thermal PMTR signal with a weakly supra-linear intensity dependence. Both types of intensity dependence were actually observed in c-Ge (Fig. 4) and in c-Si, providing unambiguous evidence that the signals measured in this work were thermally dominated. On the contrary, the im-Ge and a-Si signals were linearly dependent on intensity until saturation and transient phenomena were initiated at high powers. Therefore, the measurement of the frequency responses, $S(f)$, gave unequivocal proof that the c-Ge signal was thermally dominated, and that the im-Ge and a-Si signals had both a thermal and a trapped-carrier component. With regard to the c-Si samples, the curve-fitting of the $S(f)$ data to the theoretical model indicated that the Drude free-carrier and thermal-wave components were of similar magnitude. Furthermore, it was possible to fit all the $S(f)$ data to the theoretical model in a quantitative manner, using reasonable values for all the physical parameters (Table I) as inputs to the model. It appears that the differences between the $S(f)$ curves for the c-Si1 and c-Si2 samples were due to the much higher SRV in the c-Si2, most likely related to residual ion-implantation damage which was not completely annealed away. Thus, the PMTR technique shows promise toward quantitative imaging applications of the SRV of semiconductors.

Using the foregoing curve-fitting procedures, the goodness of the theoretical fits to the experimental frequency data such as in Figs. 5 and 6 made it possible to identify uniquely to within 20% the carrier and thermal-wave portions in each signal, by use of the composite theoretical model of §2 and the combination of literature and

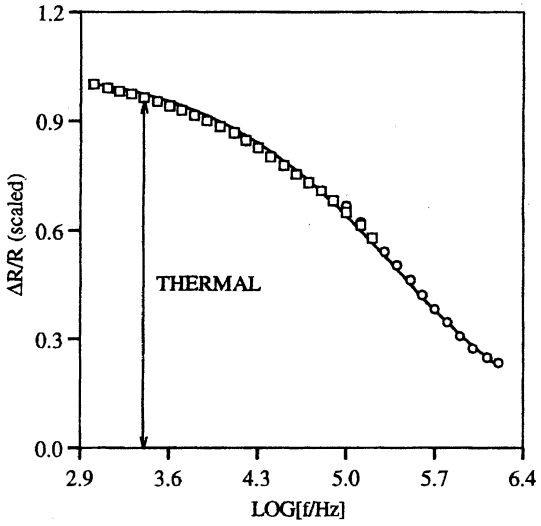

Fig. 7. PMTR amplitude vs. frequency for c-Ge. The solid line is the theoretical fit, and the squares / circles are experimental data. The fitted $1/e$ pump radius is 7.5 μm and the nominal value is 5.7 μm.

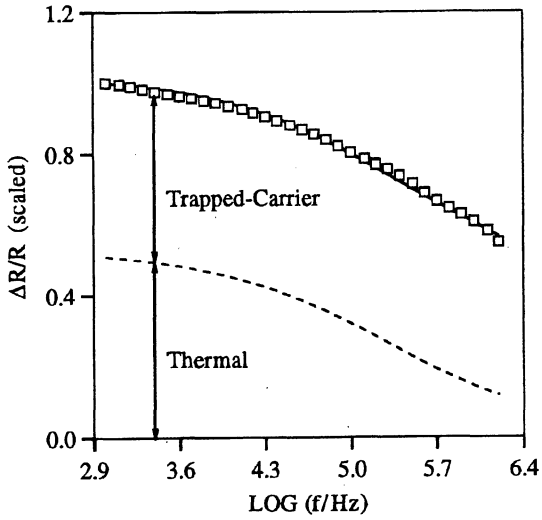

Fig. 8. PMTR amplitude vs. modulation frequency for im-Ge; the nominal $1/e$ pump radius is 5.7 μm, and the best-fit radius is 8.7 μm. The squares represent experimental data, the solid line is the theoretical fit, and the dashed line is the thermal component from theory. See Fig. 6 for further details.

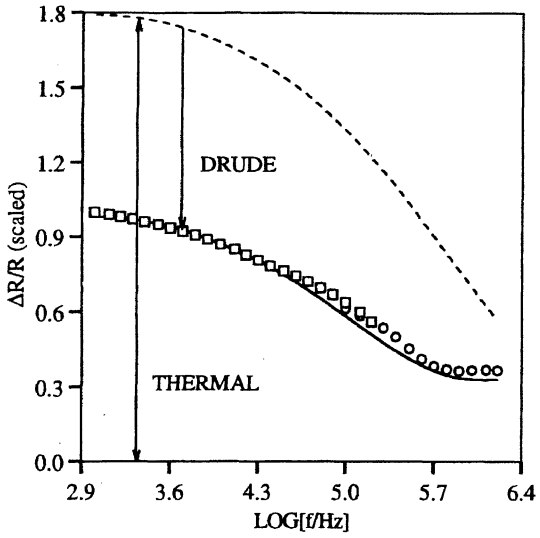

Fig. 9. PMTR amplitude vs. frequency for c-Si1. The solid line is the theoretical fit; the dashed line is the thermal component from theory; and the squares/circles are experimental data. The fitted $1/e$ pump radius is 7.0 μm and the nominal value is 5.7 μm.

experimental values shown in Tables I and III. With regard to the c-Ge sample, the curve-fitting of the $S(f)$ data to the theoretical model indicated that the thermal component was several orders of magnitude larger than the Drude free-carrier component, Fig. 7. The almost entirely thermal contribution to the signal shown in Fig. 7 is consistent with the high surface-state density known to dominate the electronic behavior of semiconductor Ge. A high surface trapping mechanism of photo-excited carriers would tend to convert the absorbed optical energy into thermal energy very efficiently, thus yielding an apparent 100% thermal transport response. For the implanted Ge sample, the thermal component was significant, but there was no significant Drude component, Fig. 8. Instead there was a signal which was hypothesized to be related to the band-filling of localized gap-states.[12–14] The trapped-carrier signal component was found to be very sensitive to the type of gaseous ambient in contact with the sample.

For the crystalline silicon materials, the thermal component was found to dominate at low frequencies, while the Drude component became quite significant near 1 MHz, especially for the larger pump spotsizes ($> 15\mu$m). Figure 9 shows a $S(f)$ curve obtained for the c-Si1 sample, exhibiting a large Drude signal component, the relative size of which grows as the frequency is increased. The change in the relative importance of the mechanisms of the PMTR signal is even more evident in the phase data, which are not presented here. The strong non-linear power law dependence of the PMTR signal on the pump intensity ($\approx I^{1.5}$) observed for c-Si1 at 10 kHz further indicates that Auger recombination effects were of some importance.[17] The c-Si2 specimen also showed both thermal and Drude character, Fig. 10, but the Drude component was less significant than for the non-implanted c-Si1 sample, consistent with the higher SRV measured for c-Si2 and the possibility of residual damage.

For the a-Si sample, the $S(f)$ data could only be fitted to the theoretical model, Fig. 11, when it was assumed that both a thermal and a carrier-related signal were present. Furthermore, it was found that acceptable fits could only be obtained when the sign of the carrier reflectance coefficient was positive. Importantly, the positive sign required for acceptable fits was consistent with theoretical modeling of the band-filling effect performed by Gay and Klauder[10] and also verified by ourselves. Overall, Fig. 11 indicates that the trapped-carrier signal component was quite large for the a-Si sample over a wide range of frequencies.

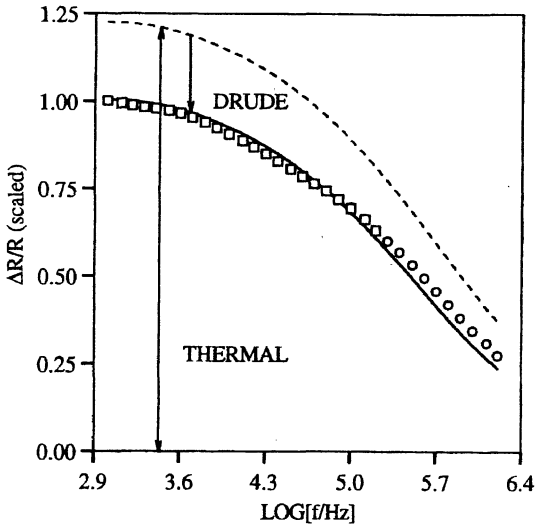

Fig. 10. PMTR amplitude vs. frequency for c-Si2. The solid line is the theoretical fit; the dashed line is the thermal component from theory; and the squares/circles are experimental data. The fitted $1/e$ pump radius is 7.1 μm, and the nominal value is 5.7 μm.

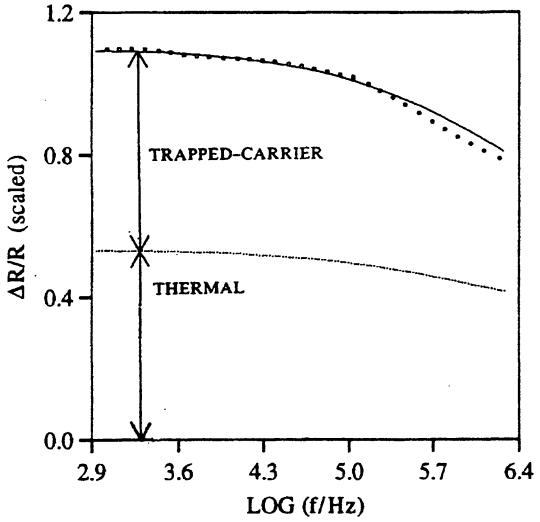

Fig. 11. PMTR amplitude vs. frequency for a-Si. The nominal $1/e$ pump radius is 5.7 μm, and the best-fit radius is 7.1 μm. The solid and dotted lines are theoretical fits. Multiplying factors to convert the PMTR amplitude to $\Delta R/R$ per Watt of absorbed power are 0.009 (experiment) and 0.0564 (theory). The absorbed pump power was 28.2 mW, and the experimental data had five cycles of smoothing.

6. Conclusions

Three-dimensional models for the PMOR signal in crystalline and ion-implanted germanium have been presented, and these models have been verified both qualitatively and quantitatively in experiments with wafer samples under well-controlled crystal growth and implantation conditions. A signal component associated with the trapped-carrier band-filling effect was hypothesized to exist in a-Si and im-Ge. The respective signal generation mechanism in the c-Ge and c-Si (unimplanted or implanted-annealed) samples was the well-known Drude effect.

A quantitative method for reconstructing the underlying components of competing electronic and thermal mechanisms contributing to the experimental PMOR data was demonstrated for the first time. The inversion method was based on quantitative determination of each component's contribution to amplitude and phase of the signal over a wide frequency range with high confidence regarding uniqueness of the vectorial-type of component addition, by determining best curve-fits to a series of frequency responses under a wide variation of pump laser beam sizes, while keeping the material parameters of the theoretical fit constant throughout the entire set of data. As a result, it was shown that c-Ge exhibits almost entirely thermal-wave contribution even under the tightest pump-beam size ($\approx 5.7\mu$m) and at the highest modulation frequencies employed in this work, while im-Ge and a-Si have significant contributions from both thermal and trapped-carrier mechanisms. Unimplanted c-Si was found to exhibit mixed Drude and thermal-wave contributions, with the former increasing in relative size with increasing frequency. Implanted and flash-annealed c-Si exhibited a similar combination of components with diminished Drude contribution, perhaps due to residual post-annealing defects. The degree of confidence in the quantitative mechanism deconvolutions from entire sets of frequency-response data under different pump-laser beam spotsizes was estimated to be no worse than 20%.

Acknowledgments

The authors wish to acknowledge the support of the Natural Sciences and Engineering Research Council of Canada (NSERC) for a Collaborative Research Grant, which made the present work possible.

1) W. L. Smith, A. Rosencwaig and D.L. Willenborg: Appl. Phys. Lett. **47** (1985) 584.
2) J. Opsal and A. Rosencwaig: Appl. Phys. Lett. **47** (1985) 498.
3) J. Opsal, M. W. Taylor, W. L. Smith and A. Rosencwaig: J. Appl. Phys. **61** (1987) 240.
4) D. Guidotti and H. M. van Driel: Appl. Phys. Lett. **47** (1985) 1336.
5) F. A. McDonald, D. Guidotti and T. M. DelGiudice: *Review of Progress in Quantitative Nondestructive Evaluation*, eds. D. O. Thompson and D. E. Chimenti (Plenum, New York, 1987) Vol. 6B, p. 1361.
6) P. Alpern, R. Kakoschke, M. Schoninger and S. Wurm,: Appl. Phys. Lett. **53** (1988) 577.
7) W. L. Smith, M. W. Taylor and J. Schuur: Proc. SPIE **530** (1985) 201.
8) L. J. Inglehart, A. Broniatowski, D. Fournier, A. C. Boccara and F. Lepoutre: Appl. Phys. Lett. **56** (1990) 1749.
9) P. Alpern, W. Bergholz and R. Kakoschke: J. Electrochem. Soc. **136** (1989) 3841.
10) J. G. Gay and L. T. Klauder, Jr.: Phys. Rev. **172** (1968) 811.
11) E. Y. Wang, W. A. Albers, Jr. and C. E. Bleil: *II-VI Semiconducting Compounds, 1967 Int. Conf. Proc.*, ed. D. G. Thomas (Benjamin, New York, 1967) p. 136.
12) L. Chen, J. Tauc and Z. Vardeny: Phys. Rev. B **39** (1989) 5121.
13) Z. Vardeny, T. X. Zhou, H. A. Stoddart and J. Tauc: Solid State Commun. **65** (1988) 1049.
14) H. Liu, D. Pfost and J. Tauc: Solid State Commun. **50** (1984) 987.
15) R. E. Wagner and A. Mandelis: J. Phys. Chem. Solids **52** (1991) 1061.
16) T. Kanata, M. Matsunaga, H. Takakura, Y. Hamakawa and

T. Nishino: Proc. SPIE **1286** (1990) 56.
17) B. C. Forget, D. Fournier and V. Gusev: Appl. Phys. Lett. **61** (1992) 2341.
18) B. C. Forget, D. Fournier and V. Gusev: Appl. Surf. Sci. **63** (1993) 255.
19) B. C. Forget and D. Fournier: Mater. Sci. Eng. B **24** (1994) 199.
20) W. H. Brattain and C. G. B. Garrett, Bell Syst. Tech. J. **35** (1956) 1019.
21) M. Vaez Iravani and H. K. Wickramasinghe: J. Appl. Phys. **58** (1985) 122.
22) J. S. Blakemore: *Semiconductor Statistics* (Dover, New York, 1987) Chaps. 5 and 6.
23) D. Fournier, A. C. Boccara, A. Skumanich and N. M. Amer: J. Appl. Phys. **59** (1986) 787.
24) G. Dearnaley, J. H. Freeman, R. S. Nelson and J. Stephen: *Ion Implantation* (North-Holland, Amsterdam, 1973) Appendix 3.
25) T. Warabisako, T. Saitoh, T. Motooka and T. Tokuyama: Jpn. J. Appl. Phys. **22** (1982) Suppl. 22-1, p. 557.
26) G. E. Jellison, Jr. and H. H. Burke: J. Appl. Phys. **60** (1986) 841.
27) Z. Vardeny, C. Thomsen and J. Tauc: Solid State Commun. **65** (1988) 601.
28) F. E. Doany, D. Grischkowsky and C.-C. Chi: Appl. Phys. Lett. **50** (1987) 460.
29) C. R. Wronski: *Semiconductors and Semimetals*, Vol. **21C**, eds. R. K. Willardson and A.C. Beer, vol. ed. J. I. Pankove (Academic, Orlando, 1984) Chap. 10.
30) W. Graf, K. Leihkamm, J. Ristein and L. Ley: *Abstr. 13th General Conf. Condensed Matter Division* (European Phys. Society, 1993) Vol. 17A, Poster SC8.4.
31) R. E. Wagner and A. Mandelis: to be published in Semicond. Sci. Technol.
32) D. E. Aspnes and A. A. Studna: Phys. Rev. B **27** (1983) 985.
33) W. G. Spitzer and H. Y. Fan: Phys. Rev. **106** (1957) 882.
34) M. Neuberger: *Group IV Semiconducting Materials* (Plenum, New York, 1971).
35) A. Mourchid, D. Hulin, R. Vanderhaghen, W. L. Nighan, K. Gzara, and P. M. Fauchet: Solid State Commun. **74** (1990) 1197.
36) D. E. Aspnes and A. A. Studna: Surf. Sci. **96** (1980) 294.
37) P. Nath and K. L. Chopra: Phys. Rev. B **10** (1974) 3412.
38) Y. C. Tai, C. H. Mastrangelo and R. Muller: J. Appl. Phys. **63** (1988) 1442.
39) A. Mandelis, R. E. Wagner, K. Ghandi, R. Baltman and P. Dao: Phys. Rev. B **39** (1989) 5254.
40) D. E. Aspnes, A. A. Studna and E. Kinsbrun: Phys. Rev. B **29** (1984) 768.
41) A. Salnick and A. Mandelis: submitted to Phys. Rev. B (1995).